MITSUBISHI ELECTRIC RESEARCH LABORATORIES
https://www.merl.com

Sizing of Electric Vehicle Power Converter Based on Distributed Operating Points

Rahman, Syed; Wang, Yebin; Menner, Marcel; Liu, Dehong

TR2024-075 June 18, 2024

Abstract

Power converters play a critical role in the operation of electric vehicles. A standard practice of power converter design is to use peak power as the operating point for power converter sizing. However, most operating points of electric vehicles are at power lower than the peak power, resulting in sub-optimal performance and overall lower efficiency in the driving life cycle. This paper presents a power converter sizing approach based on distributed operating power. The mathematical framework for this proposed approach is presented and compared with the conventional peak power design. Simulation results validate our claim.

IEEE Transportation Electrification Conference & Expo (ITEC) 2024

Mitsubishi Electric Research Laboratories, Inc.
201 Broadway, Cambridge, Massachusetts 02139

Sizing of Electric Vehicle Power Converter Based on Distributed Operating Points

Syed Rahman
Dept. of Elec. & Comp. Engr., Texas A&M University
College Station, TX, USA
syed.rahman@tamu.edu

Yebin Wang
Mitsubishi Electric Research Laboratories (MERL)
Cambridge, MA, USA
yebinwang@ieee.org

Marcel Menner
Mitsubishi Electric Research Laboratories (MERL)
Cambridge, MA, USA
marcel.menner89@gmail.com

Dehong Liu
Mitsubishi Electric Research Laboratories (MERL)
Cambridge, MA, USA
liudh@merl.com

***Abstract*—Power converters play a critical role in the operation of electric vehicles. A standard practice of power converter design is to use peak power as the operating point for power converter sizing. However, most operating points of electric vehicles are at power lower than the peak power, resulting in sub-optimal performance and overall lower efficiency in the driving life cycle. This paper presents a power converter sizing approach based on distributed operating power. The mathematical framework for this proposed approach is presented and compared with the conventional peak power design. Simulation results validate our claim.**

***Index Terms*—Electric vehicle, power converter design, multi-point optimization, peak-point design.**

I. Introduction

Long-range, improved efficiency, and fast-charging solutions are leading the path for transportation electrification. With the advancement of wide-bandgap semiconductors and high-frequency transformer technologies, it is possible to achieve higher power density and higher efficiency [1]. It also enables the operation of onboard power converters to support high-voltage motors and high-capacity batteries, as observed in the design of luxury EVs or heavy-duty trucks [2]. It is therefore desirable to optimize the design of power converters to maximize benefits from these advancements [3], [4].

However, it is very challenging to optimize the design of power converters. First, the power converter is a mix of custom-built (inductor/transformer) and off-the-shelf components (capacitors and semiconductors) [5], meaning that the design variables can be discrete and continuous. This makes it difficult to formulate the optimization problem mathematically. Second, multiple constraints make the optimization a complicated, non-convex problem. For example, besides the constraint on each variable imposed by different parameters, the overall design objective is also constrained by efficiency, cost, volume, and weight requirements [6].

To tackle the design optimization problem, most existing design approaches define an objective function based on a single point operating condition for simplicity, with constraints based on the worst-case condition, such as peak power conditions [7], [8]. These design approaches work well for peak-power drives, which operate primarily at a fixed power with a very limited power range. However, for general variable-power drives, e.g., EV propulsion drive, the peak power operation only occurs in a short time or a fraction of the whole operation period. In such a situation, this single-operating-point-based design results in sub-optimal performance since the EV usually operates at power much lower than the assumed peak power point. Therefore, it is necessary to design the power converter based on the intended operating points.

To improve the operation efficiency, optimization methods focusing on light-load efficiencies are proposed in the literature [9], [10] since light-load operations dominate the whole drive duration. Considering the overall efficiency throughout the operating range, a two-stage optimization method is proposed to optimize the power converter from light-load operations to full-load operations [11].

Following the idea of an operating-point-based design, we propose a power converter sizing approach based on the distributed operating power (DOP) probability. We formulate the design problem as an optimization problem with a cost function defined by a weighted sum of normalized efficiency, weight, and volume, subject to constraints based on the probability distribution of operating points. Compared to conventional single-operating point (peak-power) design methods, our approach yields a higher efficiency rate over practical driving life cycles. Our approach is validated by simulation results.

The rest of the paper is organized as follows. Section II discusses the power converter topology considered in this study and its parametric design. Section III defines the mathematical framework for conventional peak-point and the proposed DOP-based design methodologies, respectively, followed by simulation results in Section IV. Finally, Section V concludes the paper.

This work was done when Syed Rahman was an intern at MERL.

II. System Under Study

A. Topology

Two power electronic configurations are widely used for existing EV traction motor drives. One uses a standard three-phase DC/AC inverter, and the other includes a DC/DC converter in addition to the standard three-phase DC/AC inverter [12]. In our paper, the latter configuration is chosen for its flexibility in facilitating high-power applications. Specifically, while the first configuration is only applicable for compact-size and low-power drives, the introduction of the DC/DC converter adequately reconciles the mismatch between the need for high-power and high-voltage motor and the limited terminal voltage of the battery pack. We also note that the design idea on passive elements (inductor and capacitor) presented here can be generalized to other power electronic circuit designs where passive component parameters are critical.

A typical topology of the DC/DC/AC configuration is shown in Fig.1, which consists of a synchronous DC/DC boost converter and a three-phase DC/AC inverter using current bidirectional switches (MOSFETs with body diode). These bidirectional switches support bidirectional power flow during operations. In driving mode, the DC/DC converter boosts the battery voltage so that the DC/AC inverter generates a modulated AC voltage to operate the propulsion motor at the desired torque and speed. During regenerative braking mode, the electric power flows reversely from the motor to the battery. The DC/AC inverter works as an AC/DC rectifier, which rectifies the energy generated by the motor, and the DC/DC converter operates as a buck converter to charge the battery bank accordingly.

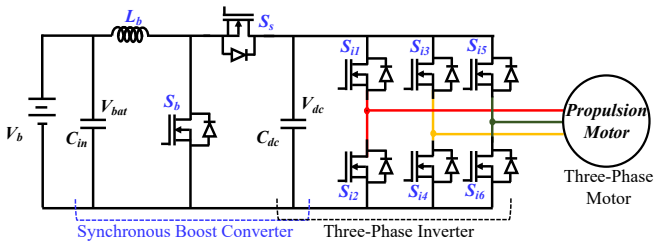

Fig. 1. Power electronic configuration showing DC/DC converter, three-phase inverter, and propulsion motor.

B. Operating Points of the Power Converters

In a typical driving cycle such as the Urban Dynamometer Driving Schedule, the operation point of the motor, e.g., the torque τ and the speed ω, varies accordingly. So does the motor's operating power. The power converter modulates the inverter output voltage magnitude and frequency to supply this power requirement. Let the operation point of motor be represented by the coordinates (τ, ω) over the torque-speed plane. For a motor given the operating power of P_m (in Watts), the line-to-line voltage V_{LL} (in Volts), and the power factor of $\cos(\phi)$, operating point parameters of the power converter are

TABLE I
Operating Points of the Power Converters

Parameter	Equation
Motor Power (P_m)	$\tau \times \omega$
Phase Current (I_{ph})	$\frac{P_m}{\sqrt{3}V_{LL}\cos(\phi)} \times \frac{1}{\eta_m}$
Modulation Index (M)	$\frac{\sqrt{2}V_{LL}}{V_{dc}}$
Avg. Link Current (I_{dc})	$\frac{P_m}{\eta_m \eta_{in} V_{dc}}$
Duty Cycle (D)	$1 - \frac{V_b}{V_{dc}}$
Link Current ($I_{c_{rms}}$) [13]	$I_{ph}\sqrt{2M\left[\frac{\sqrt{3}}{4\pi} + \cos^2(\phi)(\frac{\sqrt{3}}{\pi} - \frac{9}{16}M)\right]}$
Battery Current (I_b)	$\frac{P_m}{\eta V_b}$

calculated using equations listed in Table I, where η_m, η_{in} and η_{dc} are efficiencies of the propulsion motor, the three-phase inverter, and the DC/DC converter, respectively; V_b and V_{dc} are the battery voltage and the DC link voltage, respectively. The overall drive efficiency is given by $\eta = \eta_m \eta_{in} \eta_{dc}$.

C. Parametric Design of Components

For these operating points, equations for the parametric design are listed in Table II, where C_{in} and C_{dc} are the input capacitor and the DC link capacitor, respectively; f_s is the switching frequency; ΔI_b, ΔV_b, and ΔV_{dc} are acceptable ripple values of battery current, input voltage, and DC link voltage, respectively; $I_{b_{max}}$ and $I_{ph_{max}}$ are the battery current and the phase current while the motor is operating at rated power of P_m.

TABLE II
Minimal Parametric Values of Components [14]

Parameter	Equation
Minimum Boost Inductor ($L_{b_{min}}$)	$\frac{V_{b_{min}} D}{f_s \Delta I_b}$
Minimum Battery-Side Capacitor ($C_{in_{min}}$)	$\frac{\Delta I_b}{8 f_s \Delta V_b}$
Minimum DC link Capacitor ($C_{dc_{min}}$)	$\frac{D I_{dc}}{f_s \Delta V_{dc}}$
Minimum Boost Switch Current ($I_{sb_{min}}$)	$I_{b_{max}} + \frac{\Delta I_b}{2}$
Minimum Series Switch Current ($I_{ss_{min}}$)	$I_{b_{max}} + \frac{\Delta I_b}{2}$
Minimum Inverter Switch Current ($I_{in_{min}}$)	$\sqrt{2} I_{ph_{max}}$

III. Formulation of Optimization Problems

A. Component Modeling

As shown in Fig. 1, there are several main components to be designed: boost inductor L_b, battery-side capacitor C_{in}, DC link capacitor C_{dc}, and switching devices. The switching devices are firstly determined according to their performance and price. We focus on the design of passive components. Passive component design variables, denoted by $\mathbf{x}_c = [L_b, C_{in}, C_{dc}]^\top$, are coupled with the switching frequency f_s as shown in Table II. These design variables are related to the electrical and thermal characteristics of components, such as equivalent series resistance (ESR) and thermal resistance θ, which determine the efficiency and the temperature of power electronics.

Hence, the following considerations are taken in the modeling exercise and subsequent constraint derivation.

1) Capacitor Modeling: The capacitor is modeled as a parallel connection of multiple capacitors with an ESR R_c, where the ESR is closely related to the power loss and the corresponding temperature rise. A capacitor database is constructed to model this capacitance and its relation to other parameters.

The capacitors are then designed according to the following steps. First, given a switching frequency f_s, the minimum capacitance value is estimated using Table II. Second, the value, the total number of capacitors, and the parameters of interest, including ripple current capability I_{RMS}, ESR of capacitor R_c, thermal resistance θ_c, and capacitor volume V_c, are calculated based on the capacitance value (C_{in} or C_{dc}) and the switching frequency f_s using curve fitting according to the capacitor database.

2) Inductor Modeling: The inductor is modeled as an ideal inductor L_b connected with an ESR R_w (to be determined in the process), representing the wire resistance and accounting for the copper losses in the inductor. A pre-selected core is used for the inductor design, where the impact of permeability roll-off (due to DC magnetization bias) and the skin effect (due to switching frequency) are considered [15], [16]. The core datasheet gives vital information about the relation between various critical parameters detailed below:

- DC energy storage ($\frac{1}{2}L_bI^2$) and ampere-turns (NI),
- Ampere-turns (NI) and inductance per square turn (A_L),
- DC magnetizing force (H) and % initial permeability ($\%\mu$)), and
- Peak AC flux density (B_{pk}) and core loss (mW/cm^3).

This provided information is modeled using empirical formulae or curve fitting to establish an analytical mapping from inductance value to core losses.

In the next step, the winding resistance and weight are determined using the wire data (wire gauge, number of strands, current density, and wire density) and core data (mean length turn, winding weight). Thus, for a given f_s, using the above steps, the inductor weight and inductor losses are expressed as functions of switching frequency and inductance value, i.e., $W_{Lb}(f_s, L_b)$ and $P_L(f_s, L_b)$.

3) Switching Device Modeling: In the DC/DC converter, the SiC MOSFET is modeled as an ideal switch with a fixed series resistance (representing conduction losses) and a frequency variable series resistance (representing switching losses). The fixed resistance is obtained from the datasheet depending on the device voltage, current, and gate-source bias voltage. The variable resistance depends on the switching frequency, loss per unit switching, and operating voltage and current.

Besides the main switching devices' loss, the loss of anti-parallel diode in the SiC devices in the DC/AC inverter should also be considered in the device model. It is modeled as a resistance (representing conduction loss) in series with a voltage source (representing the cut-in voltage of the diode). Conclusively, the total device loss can be expressed as a function of switching frequency, operating current, and voltage.

Thus, when a particular switching frequency is chosen, the corresponding functions obtained from curve fitting return the power converter switch losses, inductor and capacitor losses, the inductor weight, and the capacitor volume. These values are populated in the objective function for optimization. A detailed optimization procedure is summarized in a flowchart, shown in Fig. 2.

B. Objective Functions

1) Worst Case Sizing of Power Converter: The cost function consists of a weighted sum of power losses, inductor weight, and capacitor volume. This weighted-sum-based objective function is minimized for the peak power point - worst-case design. Let the vector of design variables be $\mathbf{x} = [f_s, \mathbf{x}_c^\top]^\top$. The objective function is given by

$$f(\mathbf{x}) = P_{loss} \cdot \delta_1 + W_{Lb} \cdot \delta_2 + V_c \cdot \delta_3, \tag{1}$$

where P_{loss} is the total loss in Watt, W_{Lb} is the inductor weight in kg, and V_c is the capacitor volume in cm^3, with three impact factors δ_1, δ_2, and δ_3 on loss, weight, and volume, respectively.

The total loss P_{loss} in (1) can be expressed as

$$P_{loss} = P_{dc} + P_{inv} + P_L + P_{cap}, \tag{2}$$

where P_{dc}, P_{inv}, P_L, and P_{cap} represent the loss of DC/DC converter, inverter, inductor, and capacitor, respectively.

The DC/DC converter loss (P_{dc}) is given by [17], [18]

$$\begin{aligned} P_{dc} = &\left[I_{sb}^2 R_{DS} + E_{loss}\Big|_{I_{sb}} \cdot f_s \frac{V_{dc}}{V_{dd}}\right] N_b \\ &+ \left[I_{ss}^2 R_{DS} + E_{loss}\Big|_{I_{ss}} \cdot f_s \frac{V_{dc}}{V_{dd}}\right] N_s, \end{aligned} \tag{3}$$

where N_b and N_s present the numbers of SiC devices connected in parallel and in series, respectively, in the boost circuit, R_{DS} (in Ω) is the on-state drain to source resistance of SiC MOSFET, and E_{loss} is the switching loss per switching at operating of (V_{dd}, I_d) - given in the datasheet.

The inverter loss (P_{inv}) is given by [17]

$$\begin{aligned} P_{inv} = &6\Bigg\{ I_{in}^2 \left[R_{DS}\Big(\frac{1}{8} + \frac{M\cos\phi}{3\pi}\Big) + R_D\Big(\frac{1}{8} - \frac{M\cos\phi}{3\pi}\Big)\right] \\ &+ V_0 I_{in}\Big(\frac{1}{2\pi} - \frac{M\cos\phi}{8}\Big) + E_{loss}\Big|_{I_{in}} f_s \frac{V_{dc}}{V_{dd}}\Bigg\}, \end{aligned} \tag{4}$$

where M is the modulation index of the inverter, R_D is the on-state resistance of anti-parallel diode, and I_{in} is the peak value of output current [19].

The inductor loss, including iron core loss and copper loss, is given by an empirical formula [16]

$$P_L = I_b^2 R_w + \Big(\frac{f_s}{\frac{a}{B_{pk}^3} + \frac{b}{B_{pk}^{2.3}} + \frac{c}{B_{pk}^{1.65}}} + dB_{pk}^2 f_s^2\Big) V_{core}, \tag{5}$$

where B_{pk} is the peak AC flux density in Gauss, V_{core} (in cm^3) is the core volume, R_w (in Ω) is the wire resistance,

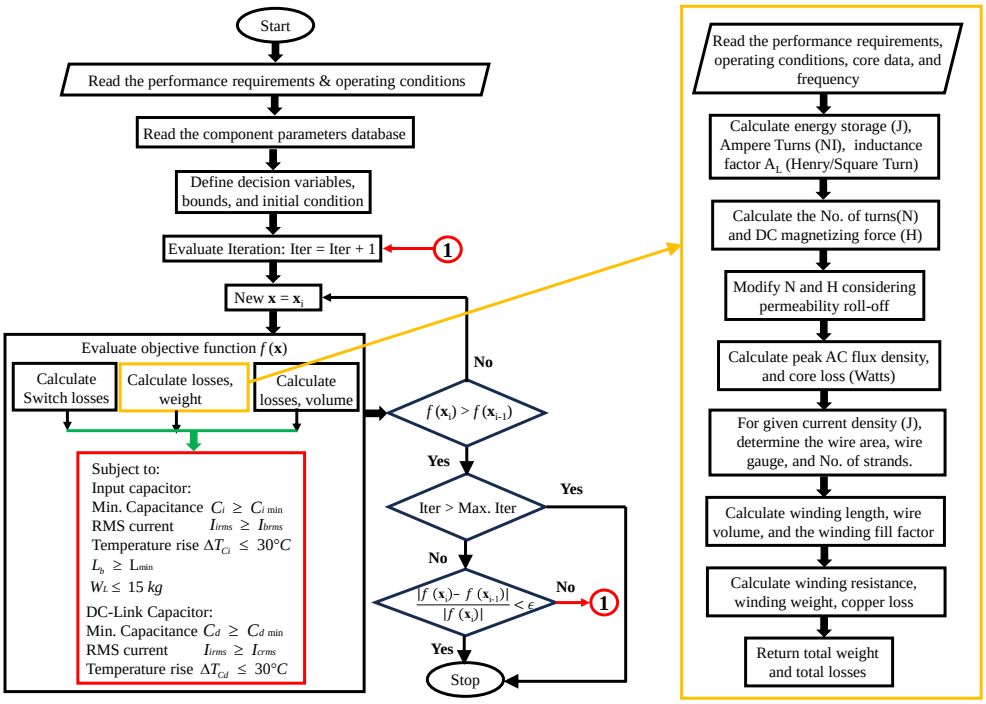

Fig. 2. Flowchart showing optimization steps along with inductor design philosophy.

and (a, b, c, d) are the coefficients obtained given in the datasheet [16].

The total capacitive loss is the sum of the DC link and input side capacitors' resistive losses, i.e.,

$$P_{cap} = I_{ci}^2 R_{ci} + I_{cd}^2 R_{cd}, \tag{6}$$

where I_{ci} and I_{cd} are RMS values of DC link capacitor and input capacitor currents, respectively, R_{ci} and R_{cd} are ESRs of the input capacitor and DC link capacitor, respectively.

The inductor weight W_{Lb} in (1) is the sum of the core weight W_{core} and the winding weight W_w, i.e.,

$$W_{Lb} = W_{core} + W_w. \tag{7}$$

The core weight W_{core} is given by the datasheet, whereas the winding weight is a function of the wire gauge, number of strands, current density, and volume of wire. The winding weight is calculated by

$$W_w = l_m \cdot A_w \cdot N \cdot \rho_{cu}, \tag{8}$$

where l_m represents the mean length turn of the wire in cm (obtained from datasheet), A_w is the area of the wire in cm^2, N is the number of wire turns on core, and ρ_{cu} is copper wire density in kg/cm^3.

The capacitor volume V_c in (1) is the sum of the DC link capacitor volume and the input capacitor volume. Given f_s, the capacitors' volume is determined using the curve fitting equation, which relates the capacitors' volume as a function of capacitor value and the number of capacitors. Mathematically, it is given by

$$V_c = N_{C_{in}}\left(a_1 \cdot C_{in}^{b1}\right) + N_{C_{dc}}\left(a_2 \cdot C_{dc}^{b2}\right) + c_1, \tag{9}$$

where $N_{C_{in}}$ and $N_{C_{dc}}$ are the numbers of input and DC link capacitors in parallel, and $(a_1, b_1, c_1, a_2, b_2)$ are coefficients obtained in the curve fitting process.

The obtained total loss, weight, and volume values are normalized for the purpose of generalization. The optimal function value with a single component (other kept zero) is determined to obtain the individual normalization factor. The next step is to select the impact factors (as defined in (1)). This selection is critical to the feasibility and conclusions drawn. This study's total loss calculations are more comprehensive than other components. For example, although the inductor weight is a significant part of the overall power converter, it should include other weights, such as capacitors and semiconductors. Similar observations can be made for the volume, wherein only capacitor volume is considered. Based on this consideration, the impact factors are selected as [δ_1, δ_2, δ_3] = [0.7, 0.2, 0.1].

2) Distributed Operating Point (DOP)-based Sizing of Power Converter: In EV operation, the operating power varies drastically for a typical driving cycle, depending upon the acceleration requirement, vehicle parameters, and road conditions. These operating points can be the basis to construct an approximate probability distribution $p(\tau, \omega)$ of operation, where τ and ω are the torque and the speed of the motor, respectively. Therefore, the DOP-based sizing has the following objective function

$$\mathrm{E}[f(\mathbf{x})] = \int_{(\tau,\omega)\in\Omega} p(\tau,\omega) f(\mathbf{x}) \mathrm{d}\tau \mathrm{d}\omega, \tag{10}$$

where $f(\cdot)$ is evaluated using (1) for a given operating point (τ, ω) over the motor's feasible domain Ω in the torque-speed plane. Note that the design variables are subject to constraints defined for each operating point. Hence, optimization (10) contains infinite constraints. Additionally, the exact evaluation of the cost function $\mathrm{E}[f(\mathbf{x})]$ is difficult, if not impossible. We propose to discretize (10) over the plane (τ, ω) so that the cost function is assessed numerically and the number of constraints is finite. Note that the computational complexity could be high with a very fine mesh size over (τ, ω).

C. Constraints

Decision variables are subjected to the following constraints.

- Capacitors: Each capacitor is constrained to be greater than the minimum capacitance and RMS current capability (calculated using Table II), with the maximum allowed capacitor temperature rise $\Delta T_{max} = 30^{\circ}$C. Mathematically, the constraints for the two capacitors are given below.
  For input side capacitor:

$$\begin{cases} C_{in} \geq \dfrac{\Delta I_b}{8 f_s \Delta V_b}, \\ I_{ci} \geq \dfrac{P_m}{\eta V_{dc}}, \\ I_{ci}^2 R_{ci} \theta_{ci} \leq \Delta T_{max}, \end{cases} \tag{11}$$

  where C_{in} is the input capacitance, I_{ci} is RMS current through the input capacitor, and θ_{ci} is the thermal resistance of the input capacitor.
  For DC link capacitor:

$$\begin{cases} C_{dc} \geq \dfrac{D I_{dc}}{f_s \Delta V_{dc}}, \\ I_{cd} \geq I_{cd_{rms}}, \\ I_{cd}^2 R_{cd} \theta_{cd} \leq \Delta T_{max}, \end{cases} \tag{12}$$

  where C_{dc} is the DC link capacitance, I_{cd} is RMS current through the DC link capacitor, and θ_{cd} is the thermal resistance of the DC link capacitor.
- Inductor: It is constrained to be greater than the minimum value, with its weight restricted by a maximum weight W_{max} =15kg. Mathematically,

$$\begin{cases} L_b \geq \dfrac{V_{b_{min}} D}{f_s \Delta I_b}, \\ W_{Lb} \leq W_{max}. \end{cases} \tag{13}$$

Moreover, the constraints can be abstracted as $\mathbf{x} \in [\mathbf{x}_L, \mathbf{x}_U]$, where $\mathbf{x}_L$ and $\mathbf{x}_U$ represent the vector of lower and upper bounds of $\mathbf{x}$, respectively.

D. Optimization Problems

Given the aforementioned component modeling, objective functions, and constraints, we are ready to formulate the optimization problems corresponding to the worst-case and DOP-based sizing. Specifically, for worst-case sizing, the optimization problem is given by $\min_{\mathbf{x} \in [\mathbf{x}_L, \mathbf{x}_U]} f(\mathbf{x})$ subjected to the constraints obtained at the peak operating point.

For the DOP-based sizing, the optimization problem is given by $\min_{\mathbf{x} \in [\mathbf{x}_L, \mathbf{x}_U]} \mathrm{E}[f(\mathbf{x})]$, where the number of constraints imposed is a function of operating points considered.

These nonlinear optimization problems can be readily coded in MATLAB® and solved using the FMINCON function. This function finds the minimum value of the multi-variable objective function, subjected to non-linear constraints [20].

IV. Simulation Validation

The parameter specifications of the EV power converter are listed in Table III. We consider both single-point-based and DOP-based designs for comparison. The same upper and lower bounds of the design variables are used in both designs, which are $\mathbf{x}_L$ = [10kHz, 50μF, 50μF, 1μH] and $\mathbf{x}_U$ = [200kHz, 1mF, 2mF, 40μH], and with the same initial values $\mathbf{x}_0$ = [200kHz, 100μF, 100μF, 40μH]. For the single-point-based design, peak power operation is considered. For the DOP-based design, a five-point-operation is considered, with per unit operating power of P = [1, 0.9, 0.85, 0.8, 0.75] and corresponding discrete probabilities p_b = [0.1, 0.15, 0.5, 0.15, 0.1].

TABLE III
Parameter Specification for the Simulation Model

Parameter	V_b	ΔV_b	V_{dc}	ΔV_{dc}	P_m
Spec	325V	0.5%	460V	1%	219kW
Parameter	ΔI_b	V_{LL}	η_i	$\cos(\phi)$	η_m, η_{dc}
Spec	15%	320V	0.98%	0.95	96%

The optimized design vectors are achieved by the single-point-based approach as $\mathbf{x}_p$ = [94.23kHz, 190μF, 618μF, 11.25μH] and by the DOP-based approach as $\mathbf{x}_d$ = [82.78 kHz, 241μF, 627μF, 11.28μH], respectively. The power, the volume, and the weight of the two designs are compared in Table IV. It is clear that the DOP-design approach achieves lower losses with a compromise in weight and volume.

TABLE IV
Comparison of the Peak-Power-Based and DOP-Based Designs

Design Approach	Peak-Power	DOP	Change
Losses at peak power [W]	8941.1	8458.7	-4.4%
Capacitor Volume [cm^3]	2188	2334	+6.6%
Inductor Weight [kg]	13.36	14.99	+12.2%

To further investigate the power loss performance, we compare the loss at different powers in Fig. 3(a) and the loss breakdown at the peak power in Fig. 3(b). It can be observed from Fig. 3(a) that with the increase of per-unit operating power, the power loss also increases, while DOP-based design results in lower power losses consistently across all the range of per-unit operating power. This is because lower switching frequency helps reduce frequency-governed losses (switching losses and core loss of inductor). This observation is also reflected in the power breakdown comparison shown in Fig. 3(b), where the DC/DC converter loss is clearly reduced for DOP-based multi-point design due to lower switching frequency.

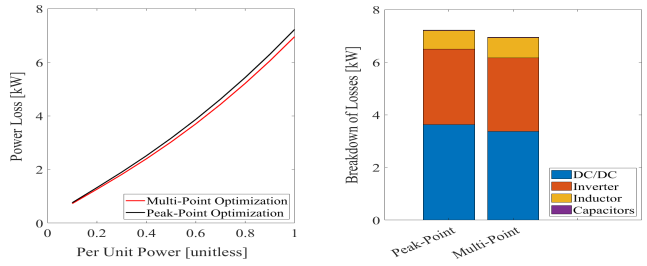

(a) (b)

Fig. 3. (a) Comparison of the power losses for different powers and (b) breakdown of losses in the two designs.

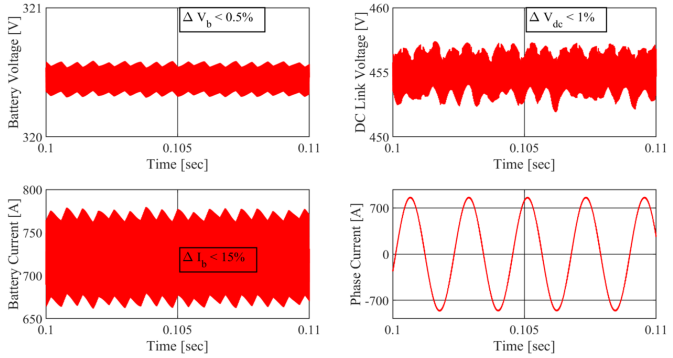

Fig. 4. Simulation results of the power converter at the peak operating power.

To verify our design, simulation is performed on a model of the power converter with optimized parameters, including (R_{DS}, R_D) of the switches, (R_{ci}, R_{cd}) of the capacitors, and R_w of the inductor. The simulation results of steady state operation are shown in Fig. 4. It can be observed that the battery voltage, battery current, and DC link signals contain DC components and ripples related to the switching frequency, while the phase current is a pure sinusoidal signal. The converter provides power to a 219kW motor at a power factor of 0.95. Further quantitative analysis shows that the ripple specifications of battery voltage, battery current, and DC link voltage meet their requirements listed in Table III as well.

V. Conclusion

This paper explored a distributed operating point(DOP)-based sizing of EV power converters. Compared to a single point (peak power)-based design, our approach considers a weighted-sum objective function with multiple operating points, their probability of operation, and individual constraints (imposed by the corresponding operating point), a practical scenario in EV driving cycles. Simulation results show that the average efficiency of the EV over the driving cycle is clearly improved. Additionally, the details related to component modeling, constraints, and the optimization method are presented. The comparison of the two design approaches shows that the DOP-based approach achieves a higher operating efficiency at the cost of a larger capacitor volume and bulky inductor. The simulation result validates that the design specifications align with the DOP-based design.

References

[1] Y. Tahir, I. Khan, S. Rahman, M. F. Nadeem, A. Iqbal, Y. Xu, and M. Rafi, "A state-of-the-art review on topologies and control techniques of solid-state transformers for electric vehicle extreme fast charging," *IET power electronics*, vol. 14, no. 9, pp. 1560–1576, 2021.

[2] U. K. Mishra, "Gallium nitride versus silicon carbide: Beyond the switching power supply," *Proceedings of the IEEE*, vol. 111, no. 4, pp. 322–328, 2023.

[3] J. W. Kolar, "Multi-objective optimization in power electronics," in *Sun-Yat-Sen-National University (NSYSU)*. ETH Zurich, 2017.

[4] R. Kondo, P. Schülting, A. H. Wienhausen, and R. W. De Doncker, "An automated component-based hardware design of a three-phase dual-active bridge converter for a bidirectional on-board charger," in *2020 IEEE Energy Conversion Congress and Exposition (ECCE)*. IEEE, 2020, pp. 850–857.

[5] S. E. De León-Aldaco, H. Calleja, and J. A. Alquicira, "Metaheuristic optimization methods applied to power converters: A review," *IEEE Transactions on Power Electronics*, vol. 30, no. 12, pp. 6791–6803, 2015.

[6] O. Bay, F. Hosseinabadi, S. Chakraborty, M. El Baghdadi, and O. Hegazy, "Multi-objective optimization of bi-directional on-board chargers based on 650v gan power transistors," in *IECON 2022–48th Annual Conference of the IEEE Industrial Electronics Society*. IEEE, 2022, pp. 1–6.

[7] W. Martinez, C. Cortes, A. Bilal, and J. Kyyra, "Finite element methods for multi-objective optimization of a high step-up interleaved boost converter," in *2018 International Power Electronics Conference (IPEC-Niigata 2018-ECCE Asia)*. IEEE, 2018, pp. 2193–2198.

[8] S. Busquets-Monge, G. Soremekun, E. Hefiz, C. Crebier, S. Ragon, D. Boroyevich, Z. Gurdal, M. Arpilliere, and D. K. Lindner, "Power converter design optimization," *IEEE Industry Applications Magazine*, vol. 10, no. 1, pp. 32–38, 2004.

[9] O. Trescases and Y. Wen, "A survey of light-load efficiency improvement techniques for low-power dc-dc converters," in *8th International Conference on Power Electronics-ECCE Asia*. IEEE, 2011, pp. 326–333.

[10] Y. Jang and M. M. Jovanovic, "Light-load efficiency optimization method," *IEEE Transactions on Power Electronics*, vol. 25, no. 1, pp. 67–74, 2009.

[11] R. Yu, B. M. H. Pong, B. W.-K. Ling, and J. Lam, "Two-stage optimization method for efficient power converter design including light load operation," *IEEE Transactions on Power Electronics*, vol. 27, no. 3, pp. 1327–1337, 2011.

[12] J. Reimers, L. Dorn-Gomba, C. Mak, and A. Emadi, "Automotive traction inverters: Current status and future trends," *IEEE Transactions on Vehicular Technology*, vol. 68, no. 4, pp. 3337–3350, 2019.

[13] D. Cittanti, F. Stella, E. Vico, C. Liu, J. Shen, G. Xiu, and R. Bojoi, "Analysis and design of a high power density full-ceramic 900 v dc-link capacitor for a 550 kva electric vehicle drive inverter," in *2022 International Power Electronics Conference (IPEC-Himeji 2022-ECCE Asia)*. IEEE, 2022, pp. 1144–1151.

[14] B. Hauke, "Basic calculation of a boost converter's power stage," *Texas Instruments, Application Report November*, pp. 1–9, 2009.

[15] "Inductor design with magnetics powder cores," https://www.mag-inc.com/Design/Design-Guides/Inductor-Design-with-Magnetics-Powder-Cores, accessed: 2023-07-21.

[16] "Fs-775026-2 datasheet," https://datasheets.micrometals.com/FS-775026-2-DataSheet.pdf, accessed: 2023-07-21.

[17] D. Graovac, M. Pürschel, and A. Kiep, "Mosfet power losses calculation using the datasheet parameters," *Application Notes 2006-07 V1.1*, pp. 1–23, 2006.

[18] E. Gurpinar and B. Ozpineci, "Loss analysis and mapping of a sic mosfet based segmented two-level three-phase inverter for ev traction systems," in *2018 IEEE Transportation Electrification Conference and Expo (ITEC)*. IEEE, 2018, pp. 1046–1053.

[19] "SCTW100N65G2AG datasheet," https://www.st.com/resource/en/datasheet/sctw100n65g2ag.pdf, accessed: 2023-07-21.

[20] Mathworks, "Find minimum of constrained nonlinear multivariable function - matlab fmincon." [Online]. Available: https://www.mathworks.com/help/optim/ug/fmincon.html?s_tid=doc_ta